Mechanical Systems and Signal Processing 224 (2025) 112219

Contents lists available at ScienceDirect

Mechanical Systems and Signal Processing

journal homepage: www.elsevier.com/locate/ymssp

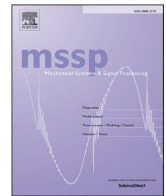

Invited for the Special Issue in Honor of Professor John Mottershead

# Real-time monitoring of thin film thickness and surface roughness using a single mode optical fiber

Fengfeng Zhou [a], Siying Chen [a], Semih Akin [b], Theodore Gabor [a], Martin B.G. Jun [a,*]

[a] School of Mechanical Engineering, Purdue University, 585 Purdue Mall, West Lafayette 47907-2088, USA
[b] Department of Mechanical, Aerospace and Nuclear Engineering, Rensselaer Polytechnic Institute, Troy, NY 12180, USA

ARTICLE INFO

*Keywords:*
Thin film monitoring
Real-time monitoring
Surface roughness
Optical fiber sensor
Fabry-Perot interferometer

ABSTRACT

This research introduces an innovative method for real-time monitoring thin film growth and surface roughness using a single mode optical fiber without any additional treatment. The cleaved end of the fiber was installed within the deposition chamber, allowing the thin film to be deposited directly onto the fiber tip. During the deposition process, a Fabry-Pérot interferometer was formed with its cavity length equal to the film thickness. As the thin film grows, it alters the cavity length, resulting in a measurable interferogram. In cases where the film surface is not optically smooth, surface roughness becomes a function of deposition time. By leveraging this phenomenon, this research demonstrates a method for calculating film thickness and surface roughness using Hilbert Transform along with an iterative method. It was found that the measured film thickness fluctuates around the ground truth given by a simulation, with an error on the nanometer scale ($\leq$4 nm) and the reflectivity error is less than 0.004 (maximum error percentage of 5.86 %). Compared to traditional quartz crystal microbalance counterpart, the proposed method directly measures the film thickness rather than mass of the thin film. Furthermore, the compact probe design allows it to be placed closer to the substrate, enhancing monitoring precision. This method offers a simple, quick, and affordable approach to monitor film thickness and surface roughness, effectively addressing the current challenges in the field.

## 1. Introduction

Thin film technologies promote the flourishing of semiconductors [1–3], optics [4–6], functional materials [7–9], and other fields [10–12] due to their unique electrical, optical, and mechanical properties [13–15]. Control of thin film growth process becomes essential as the integration level of semiconductor devices drastically increases and the requirements to thin films become more diverse. Monitoring of thin film growth is necessary to achieve effective control of the deposition process, improving the quality and yield of thin film products. In this regard, a real-time monitoring system, typically quartz crystal microbalance (QCM), is usually used to measure the mass of the material deposited on its surface [16–18]. However, QCM measures the mass rather than the thickness directly. Additionally, QCMs are relatively bulky and cannot be installed close enough to the substrate without affecting the deposition process. Optical methods, such as incremental dielectric reflection, have also been developed to monitor film growth [19]. This method

*Notations:* ALD, atomic layer deposition; EMD, Empirical Mode Decomposition; FPI, Fabry-Pérot Interferometer; FSR, free spectrum range; HT, Hilbert Transform; QCM, quartz crystal microbalance; SMF, single mode optical fiber.

* Corresponding author.
*E-mail address:* mbgjun@purdue.edu (M.B.G. Jun).

https://doi.org/10.1016/j.ymssp.2024.112219
Received 27 August 2024; Received in revised form 2 December 2024; Accepted 5 December 2024
Available online 14 December 2024
0888-3270/© 2024 Elsevier Ltd. All rights reserved, including those for text and data mining, AI training, and similar technologies.

relies on monitoring the reflectance of the polarized light slightly off the Brewster angle (i.e., the reflection angle perpendicular to the refraction angle). As such, careful preparation of the optical system is needed for the monitoring using this approach, which subsequently increases the overall process cost.

Unlike the QCM, optical fiber sensors use light as the sensing resource and can employ either modified or unmodified optical fiber as the sensing structure [20–23]. These sensors are compact in size [24,25], resistant to harsh environments [26], highly sensitive [27–29], and immune to electromagnetic interference [30], thereby offering significant potential for high-fidelity monitoring thin-film growth without the need for additional treatment. Furthermore, optical fiber interferometers can easily reach an accuracy and precision of sub-nanometer scale for distance/thickness measurement, making them ideal for high precision monitoring. Among the most widely used configurations, optical fiber Fabry-Pérot interferometers (FPIs) feature a simple structure, a high signal to noise ratio, and a high finesse [31]. Owing to these characteristics, optical fiber FPI has a remarkable potential for thin film growth monitoring, as it provides the optical thickness of the thin film with its compact diameter of 125 μm. However, the free spectrum range (FSR) of the interference spectrum of an FPI is determined by its cavity length. As the thin film grows from zero thickness, there occurs a loss of data at the beginning of the process because the FSR is greater than the wavelength range of the spectrometer for the methods based on the interference spectrum [24].

To address the above-mentioned challenges, this study introduces a method using a single mode optical fiber (SMF) to monitor the growth process of thin films, including film thickness and surface roughness. As shown in Fig. 1, an SMF with a cleaved end was installed into the deposition chamber of an atomic layer deposition (ALD) system. When the thin film is deposited on the tip of the SMF, the interfaces between the SMF and the thin film, as well as the thin film and the vacuum/gas form an FPI. As the film thickness changes, the intensity of the light reflected by the FPI varies due to multibeam interference. However, the surface roughness of the interface between the film and the vacuum/gas can change due to an imperfect deposition process, deforming the interferogram. To mitigate this uncertainty, Hilbert Transform (HT) was used to calculate the instantaneous phase, and consequently the thin film thickness. To improve the accuracy, we refrained from assuming two-beam interference as it may cause additional errors since the material of the film used in the experiment has a high reflectivity compared to vacuum/gas. In this paper, we demonstrate that the film thickness and the instantaneous phase given by HT is a one-to-one mapping, ensuring the uniqueness of the film thickness derived from the instantaneous phase. Furthermore, we provide a method to calculate the film thickness when the reflectivity of the film-vacuum/gas interface changes during the deposition process. We also evaluate the error by simulating a deposition process with changing film-vacuum/gas interface reflectivity, showing that the error is in a nanometer scale. Other than film thickness, the reflectivity of the film-vacuum/gas interface can also be calculated from the interferogram. The proposed method requires no special treatment of the SMF, which makes it affordable, time efficient, and easy to fabricate, thereby offering the potential for the emerging fields such as optical coating monitoring, semiconductor manufacturing, etc.

## 2. Method

Consider a problem that consists of three different materials labeled as 1, 2, and 3 as shown in Fig. 2 with refractive indices of $n_1$, $n_2$, and $n_3$, respectively. This setup forms two interfaces, labeled as Interface 1 and Interface 2. In this analysis, the scattering of Interface 1 and the absorption of material 2 will be ignored. The scattering of Interface 2 will be considered as shown in Fig. 2. Given that we only

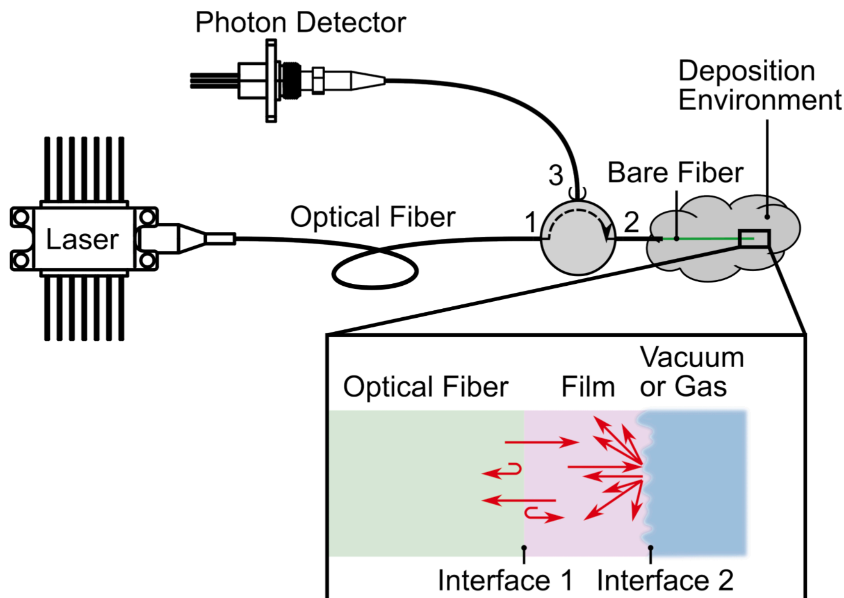


**Fig.1.** Schematic of the thin film growth monitoring method.

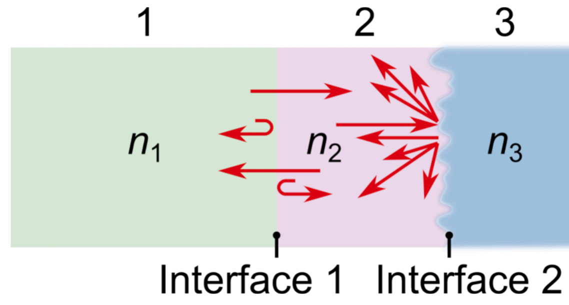


**Fig.2.** Schematic of the loss of reflection intensity caused by scattering.

consider the reflected light propagating along the opposite direction to the incident light, the scattering is equivalent to a reduction in reflection of Interface 2. Assume that material 2 is a thin film deposited on a substrate (i.e., material 1), and material 3 is the vacuum or gas environment. The surface roughness of Interface 2 changes during the deposition process; therefore, the reflectivity $R_2$ will be a function of deposition time. Utilizing this phenomenon, an FPI can be established to high-fidelity monitoring of thin film growth and surface roughness.

In this regard, Ismail *et al.* [32] analyzed the property of FPIs, and the reflection intensity of an FPI can be written as:

$$I_r = 1 - \frac{T_1T_2}{1 + R_1R_2 - 2\sqrt{R_1R_2}\cos\varphi}, \# \tag{1}$$

where $R_i$ is the reflectivity of Interface $i$, $T_i$ is the transmissivity of Interface $i$, $\varphi = 4\pi n_2 l_0/\lambda_0$ is the phase change when light travels between Interface 1 and Interface 2 for a roundtrip, $l_0$ is the geometric distance between Interface 1 and Interface 2, and $\lambda_0$ is the wavelength of the light in vacuum. Here, we assume $n_2 > n_1$ and $n_2 > n_3$ to match the condition of our experiment, the reflection phase change when incident light is reflected by interface 1 was considered in Eq. (1). Let $a = 1$, $b = -T_1T_2$, $c = 1 + R_1R_2$, $d = 2\sqrt{R_1R_2}$, and $s = 4\pi n_2/\lambda_0$ for simplicity, Eq. (1) can be rewritten as:

$$I_r(l_0) = a + \frac{b}{c - d\cos(sl_0)}.\# \tag{2}$$

Eq. (2) is a periodic function due to the term $\cos(sl_0)$. Consider the definition of Hilbert transform that shifts all the positive frequency components of the original signal for $-\pi/2$ and all the negative frequency components of the original signal for $\pi/2$. The Hilbert transform of Eq. (2) is:

$$\widetilde{I}_r = a + \frac{b}{c - d\sin(sl_0)}.\# \tag{3}$$

Therefore, the analytical spectrum of the reflection spectrum is:

$$I = I_r + i\widetilde{I}_r, \# \tag{4}$$

where $i$ is the imaginary unit. The Intrinsic Mode Function (IMF) of Eq. (4) is given by:

$$g = a + \frac{b}{c}.\# \tag{5}$$

Hence, the analytical spectrum becomes:

$$\begin{cases} I'(l_0) = \dfrac{b}{c - d\cos(sl_0)} - \dfrac{b}{c} \\ \widetilde{I}'(l_0) = \dfrac{b}{c - d\sin(sl_0)} - \dfrac{b}{c} \end{cases}.\# \tag{6}$$

The instantaneous phase becomes:

$$p = \angle A_c' = \arctan\left[\frac{c - d\cos(sl_0)}{c - d\sin(sl_0)}\tan(sl_0)\right].\# \tag{7}$$

Take derivative of instantaneous phase $p(x)$ with respect to $x$, where $x = sl_0$. We have:

$$\frac{dp}{dx} = \frac{d\sin(x)\tan(x)[c - d\sin(x)] + \sec^2(x)[c - d\cos(x)][c - d\sin(x)] + d[c - d\cos(x)]\sin(x)}{[c - d\sin(x)]^2 + \tan^2(x)[c - d\cos(x)]} > 0.\# \tag{8}$$

Therefore, instantaneous phase increases monotonically with respect to the geometric thickness of material 2. So, the mapping between the geometric thickness $l_0$ and the instantaneous phase $p$ is a bijection, which guarantees we can always back calculate the thickness of material 2 from its instantaneous phase.

Rewrite Eq. (1), we have a function $g(l_0)$ such that:

$$h(l_0) = \frac{R_1 - I_r}{2(1-I_r)\sqrt{R_1}}\frac{1}{\sqrt{R_2}} + \frac{1-R_1 I_r}{2(1-I_r)\sqrt{R_1}}\sqrt{R_2} = \cos(s l_0).\# \quad (9)$$

So, $h(l_0)$ maps the interferogram into a cosine function. In this case, the geometric thickness of material 2 can be calculated from the instantaneous phase of function $h(l_0)$.

However, in some applications, the surface roughness of material 2 may change during the deposition process. This change in surface roughness introduces additional loss when light is reflected by Interface 2. Consequently, this extra loss can be treated as a change in $R_2$ throughout the deposition process. As such, it is necessary to investigate how $R_2$ affects the instantaneous phase.

Consider the deposition $TiO_2$ thin film (refractive index $n_2 = 2.4328$ at 1550 nm [33]) on an optical fiber (core refractive index $n_1 = 1.4440$ at 1550 nm [34,35]). Assume the refractive index of vacuum/gas $n_3 = 1.0000$. Then, the reflectivity of Interface 1 is $R_1 = 0.0651$, and the reflectivity of interface 2 is $R_2 = 0.17421$. During the deposition process, the reflectivity of Interface 2, noted as $R_2$, deviate from that with an optical smooth interface $R_{20}$. When calculating the film thickness, Interface 2 can be assumed as optically smooth. Under these assumptions, Eq. (9) becomes:

$$h_r = \frac{R_1 - I_e}{2(1-I_r)\sqrt{R_1}}\frac{1}{\sqrt{R_{20}}} + \frac{1-R_1 I_e}{2(1-I_r)\sqrt{R_1}}\sqrt{R_{20}},\# \quad (10)$$

where $R_{20}$ is the reflectivity of Interface 2 with optical smooth, $R_2$ is the reflectivity deviates to $R_{20}$, and $I_e$ is the experimental interferogram. To assess the error caused by this incorrect assumption, we calculated the theoretical reflection intensity $I_r$ using Eq. (1) with different $R_2$. Then, we calculated $h_r$ by letting $I_e = I_r$ in Eq. (10). It should be noted that in Eq. (10) we used $R_{20}$ instead of $R_2$ to simulate that we use an incorrect reflectivity of Interface 2. Fig. 3 shows the error introduced by incorrect $R_2$. When $R_2 = R_{20} = 0.17421$, the error is zero since it satisfies our assumption. However, when the value is greater or smaller than this value (usually smaller due to the scattering), the maximum error of the thickness $l_0$ will increase with the increase in the error of $R_2$. When the optical thickness of material 2 equals an integer multiple of a quarter of the wavelength of the light, the error will approach zero.

However, the film thickness and the reflectivity were calculated based on the assumption that Interface 2 is optically smooth, which introduces error in the results. To reduce this error, we introduce an iterative method. From Eq. (10), we calculate the thin film thickness by applying HT. Therefore, the film thickness should be:

$$l = p_i / s,\# \quad (11)$$

where $p_i$ is the instantaneous phase given by HT. Then, according to Eq. (A14) in Appendix, $R_2$ can be calculated. The calculated $R_2$ will be closer to the true reflectivity of Interface 2 compared to $R_{20}$ that we used in Eq. (10). Therefore, we will replace $R_{20}$ in Eq. (10) with the calculated $R_2$ for the second round of calculation. This process will be repeated multiple times until there is no significant improvement of the results. We will illustrate this iteration method and discuss the error in the next section.

Knowing the reflectivity of the film-vacuum/gas interface, the surface roughness of the film can be effectively estimated. In our case, both specular and diffusion reflection of normal incidence are considered at the film-vacuum/gas interface. Therefore, the reflectivity can be simplified to the following form for wavelength at 1550 nm (considered as long wavelength in this model and therefore the diffuse reflection term can be ignored) [36]:

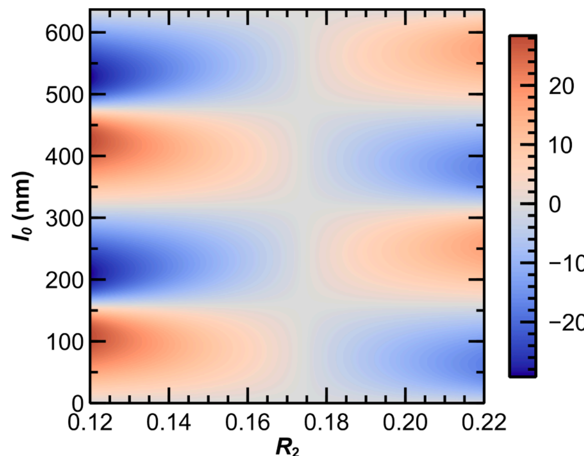


**Fig.3.** Influence of $R_2$ on the thickness error of Material 2.

$$\sigma = \frac{\lambda}{4\pi}\sqrt{\ln\frac{R_0}{R_s}}, \# \tag{12}$$

where $R_0$ is the reflectivity for smooth reflection surface and $\sigma$ is the root mean square surface roughness.

## 3. Results and discussion

The ALD process is a chemical deposition method which repetitively deposits one single layer of atoms on the substrate. In this experiment, the process to deposit one atomic layer includes the following steps:

Step 1. Fill up the deposition chamber with $TiCl_4$ vapor.
Step 2. Purge the deposition chamber with $N_2$ gas.
Step 3. Fill up the deposition chamber with $H_2O$ vapor.
Step 4. Purge the deposition chamber with $N_2$ gas.

These 4 steps form a cycle that will generate one single atomic layer, and multiple layers can be deposited by repeating this cycle.

### 3.1. Numerical test and error Discussion

To demonstrate the process of the iteration method, we implemented a numerical test. Assume we deposit a thin film on an SMF with a refractive index of $n_2 = 2.4328$ at 1550 nm. The wavelength of the monitoring light was also set to 1550 nm. To simulate the deposition process, the growth rate and the reflectivity of Interface 2 were obtained from one experimental data based on our experience. The growth rate follows the function:

$$v(C) = \frac{v_M}{2}\{\tanh[p_d(C - q_d)] + 1\}, \# \tag{13}$$

where $v$ is the growth rate with a unit of nanometer per cycle, $v_M = 0.061\text{nm/cycle}$ is the maximum growth rate, $p_d = 2\times10^{-4}$ and $q_d = 2\times10^{-3}$ are two parameters that determines the growth process, and $C$ is the cycle number. Then the thickness becomes:

$$l_0(C) = \int_0^C \frac{v_M}{2}\{\tanh[p_d(x_C - q_d)] + 1\}dx_C = \frac{v_M}{2}\left\{\frac{1}{p_d}\ln\frac{\cosh[p_d(C - q_d)]}{\cosh(-p_d q_d)} + C\right\}. \# \tag{14}$$

Assume the reflectivity $R_2$ follows the function:

$$R_2 = R_{20}e^{-C/w}, \# \tag{15}$$

where $w = 12000$. Fig. 4 a) shows the growth rate and the reflectivity of Interface 2 changes with cycle number during film growth based on the assumptions. As we can see, the growth rate increases gradually and reaches a relatively stable value at around 0.06 nm/cycle. For $R_2$, we assume that due to the increase of the surface roughness during the deposition, the reflectivity of Interface 2 will reduce gradually. Fig. 4 b) shows the interferogram based on the assumptions. The optical thickness will increase with an increase of the cycle number and therefore the reflection intensity will change periodically with the increase of the cycle number under ideal conditions. However, because of the change of the reflectivity of the $TiO_2$ interface $R_2$, the reflection intensity of the peaks will not equal. The cycle numbers between two adjacent minimums are different due to the nonconstant growth rate. Also, because of the reduction of $R_2$, the values of maxima and minima also decrease with an increasing cycle number. This interferogram can be used to simulate the experimental condition and evaluate the error in the film thickness calculated using the proposed method.

Since the interferogram is an Airy function, which includes a cosine function in the denominator as given in Eq. (1), calculating the instantaneous phase directly would introduce extra error. Therefore, we need to transform the interferogram to Eq. (10) to reduce this

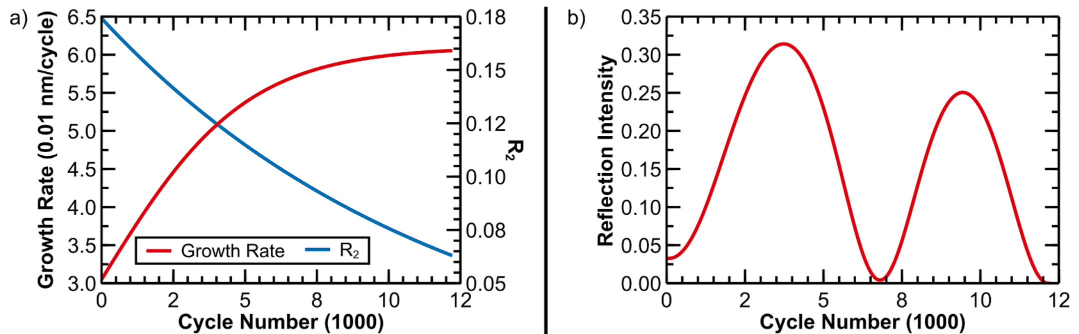


**Fig.4.** Deposition process of a thin film on an optical fiber. a) growth rate change, reflectivity of Interface 2, and b) the induced reflection intensity with cycle number.

error. However, since we use $R_{20}$ instead of $R_2$ in Eq. (10), the transformed interferogram will not be a perfect cosine function as shown in Eq. (9). Instead, due to the change of $R_2$, the amplitude will deviate from the cosine function, causing the area above and below $g_r(l_0)$ not equal to zero. To address this, we need to apply Empirical Mode Decomposition (EMD) before performing HT [37]. This will yield instantaneous frequency. With the instantaneous phase, the film thickness can be estimated using:

$$l_{0r} = p_i/s, \# \tag{16}$$

where $p_i$ is the instantaneous phase given by the HT. Here, we need to notify that Eq. (16) comes from Eq. (9), whereas the instantaneous phase is calculated from Eq. (10). Therefore, the film thickness given by Eq. (15) contains error which is caused by using $R_{20}$ instead of $R_2$ in Eq. (10). This error causes the deviation of the instantaneous amplitude from 1.

Fig. 5 shows the exact thickness of the film (labeled as Ground Truth) and that calculated using the proposed method (labeled as Measured Thickness). As shown in Fig. 5, the measured thickness matches the true thickness well. The green curve represents the difference between the measured thickness and the true thickness (Measured Thickness minus True Thickness). We can see that the error oscillates around zero, with the points near the maxima and minima in the interferogram being close to zero. This roughly agrees with the conclusion given by Fig. 3. The difference arises because in Fig. 3 we assume the deviation of $R_2$ from $R_{20}$ is constant, whereas in real conditions this deviation changes with the deposition process of the thin film. Nonetheless, the film thickness at the maxima and minima of the interferogram is generally more precise than at other points.

By knowing the film thickness, we can also evaluate the growth rate given by HT by taking the derivative of the film thickness. It should be noted that taking the derivative will amplify the noise, therefore for experimental data, a smooth process of the film thickness curve is usually needed before calculating the growth rate. Fig. 6 shows the exact growth rate (labeled as Ground Truth) and that given by HT (labeled as Measured Growth Rate). The difference between the true and the measured growth rate becomes significant. The measured value fluctuates around the true value. This difference arises from the same source as the error in the film thickness.

Since the film thickness is known, it is also possible to estimate the reflectivity of Interface 2 using Eq. (9). The details about the existence and how to choose solutions are given in Appendix A. Fig. 7 shows the ground truth of $R_2$ and that measured by HT. As we can see, the measured value oscillates around the ground truth with an error lower than 0.01. This error is because of our incorrect assumption that the reflectivity of the thin film-vacuum/gas interface does not change. However, even with some error, the $R_2$ given by Fig. 7 is better than our assumption that $R_2 = R_{20}$. Therefore, we can try to substitute the $R_2$ given by Fig. 7 into Eq. (9) to recalculate film thickness $l_0$ and the reflectivity $R_2$ again follow the same process to improve the accuracy. This process will be repeated for multiple times until no significant $l_0$ and $R_2$ can be observed.

We also tested how the iteration will affect the error. It should be noted that after calculating the $R_2$ for each iteration, we use the values of $R_2$ at each maximum or minimum in the interferogram to avoid divergence. This is because the result is very sensitive to $R_2$ and those points at maxima or minima have the least error. After obtaining the values at the maxima and minima, linear interpolation was applied to get $R_2$ at all sampling points for further calculations. Fig. 8 shows he maximum difference in film thickness compared with the ground truth and the last iteration for different iteration numbers. The inset shows the detail between iteration number 30 and 38. As we can see at the beginning, the maximum iteration compared with the ground truth was −3.5881 nm. At the second iteration, the difference was immediately reduced to −2.5982 nm. After that, the difference shows a periodic fluctuation between −2.6050 nm and −2.6064 nm. Therefore, under this condition, the error converges after two iterations. More iterations will not improve accuracy. However, considering that in the real monitoring process the ground truth is unknown, we need to consider the maximum difference of the film thickness between the current and the last iteration. As we can see from Fig. 8, the first difference is zero because there is no previous film thickness to compare with. Starting from the second iteration, the difference quickly reduced from −1.2404 nm to −0.0083 nm. After that, the difference fluctuated periodically between 0.0014 nm and −0.0014 nm with a similar period and phase compared with the ground truth. Therefore, by observing the difference compared with the last iteration, we can also determine if the

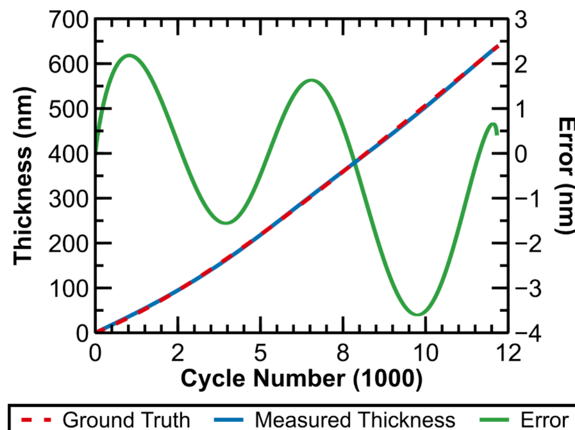


**Fig.5.** Comparison between the exact film thickness (True Thickness) and that measured using Hilbert Transform (Measured Thickness).

 

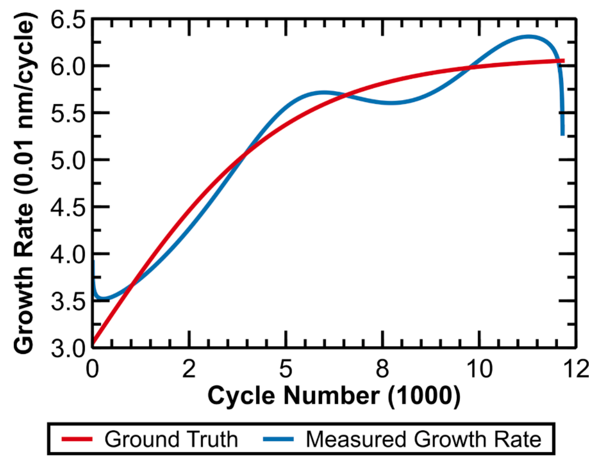


**Fig.6.** Comparison between the exact growth rate (True Growth Rate) and that measured using Hilbert Transform (Measured Growth Rate).

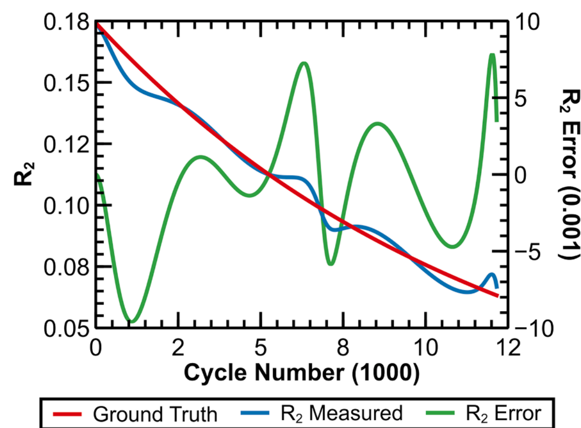


**Fig.7.** Comparison between the exact reflectivity ($R_2$ True) and that the reflectivity measured using Hilbert Transform ($R_2$ Measured).

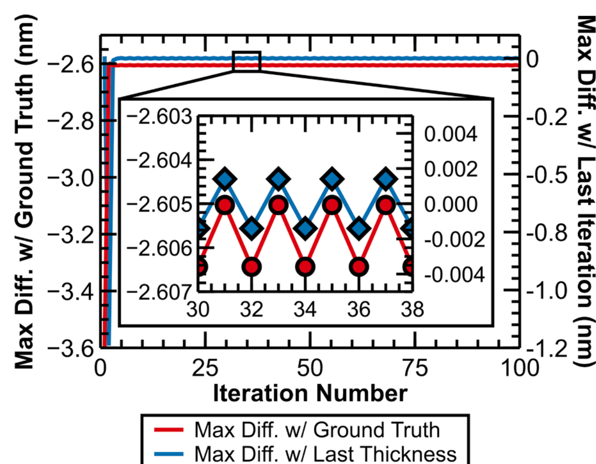


**Fig.8.** Maximum difference in film thickness compared to the ground truth and last iteration.

result converges or not.

Fig. 9 a) shows the error of iteration 1 and iteration 100 with the ground truth. For iteration 100, the maximum error was reduced to 2.6064 nm compared with 3.5881 nm for the first iteration. Generally, after 100 iterations, the error still fluctuates around the ground

truth with lower amplitude. Fig. 9 b) shows the growth rate of the ground truth, iteration 1, and iteration 100. Both growth rates for iteration 1 and 100 wiggles around the ground truth. For iteration 100, the growth rate is generally closer to the ground truth than that of iteration 1, except for some outliers. These outliers are the discontinuity of the first order derivative when subsampling and linearly interpolating $R_2$ during the iteration. However, these outliers are easily identifiable and can be removed if a smooth change of the growth rate is assumed. Fig. 9 c) shows $R_2$ for iteration 1 and iteration 100. For iteration 100 the reflectivity is closer to the ground truth, and the maximum error reduced to 0.0039, compared to that of iteration 1 (~0.01). As such, iteration improves quickly and reduces the error for both film thickness and reflectivity of Interface 2.

### 3.2. Monitoring of $TiO_2$ thin film growth

Fig. 10 shows the ALD and the monitoring system setup. The cleaved end of an SMF was installed in an ALD system to monitor the thin film growth process. The inset shows the $TiO_2$ film deposited on the tip of the SMF, which forms two reflection surfaces (Interface 1 and Interface 2). Interface 1 is the interface between SMF and the thin film material ($TiO_2$ here), and interface 2 is the interface between the thin film material and the vacuum/gas. These two reflection interfaces form an FPI, causing multibeam interference between the interfaces. $TiCl_4$ and $H_2O$ were used as precursors to deposit $TiO_2$ thin film, with $N_2$ gas being used as the carrier gas. A beam of laser with a wavelength of 1550 nm was injected into the SMF and the reflected light was guided to a photodetector using an optical circulator. Therefore, the reflected light can be recorded throughout the deposition process.

The deposition recipes for different tests were shown in Table 1 [38]. Tests 4 and 5 were conducted with the same processing parameters. Dose 1 was $TiCl_4$, and dose 2 was $H_2O$. Tests 8 and 9 have a higher pressure due to the reaction between $TiCl_4$ and the vacuum pump oil reduced its performance. The furnace temperature was also set higher as test 4 and 5. For test 8, the duration of dose 2 was increased to 0.5 sec. For test 9, the duration of the purges was reduced to 1.5 sec compared with test 8.

Fig. 11 shows the monitoring reflected light intensity detected by the photodetector. The refractive index of $TiO_2$ thin film at 1550 nm is 2.4328 [33]. Before deposition, there is only one reflection surface, known as the interface between the SMF and the vacuum. After the deposition starts, multibeam interference will occur between the two interfaces. And the reflection intensity increases until it reaches the maximum point which is caused by the constructive interference. Since the change of $R_2$ will not affect the maximums and minimums as shown in Appendix B. At the maximum point, the optical thickness of the film is $\lambda/4$ due to the constructive interference requirement, $\lambda$ is the wavelength of the light. After reaching the maximum point, with the increase of the film optical thickness, the reflection intensity gradually decreases because the optical thickness of the film deviates from the constructive interference to the destructive interference condition. Then, the reflection intensity will reach a minimum value of which the optical thickness of the film satisfies the destructive interference condition. At this point the optical thickness of the thin film equals to $\lambda/2$. This process will repeat, and the second maximum will appear at $3\lambda/4$ and the second minimum will appear at $\lambda$. Fig. 11 also shows the geometric thickness at

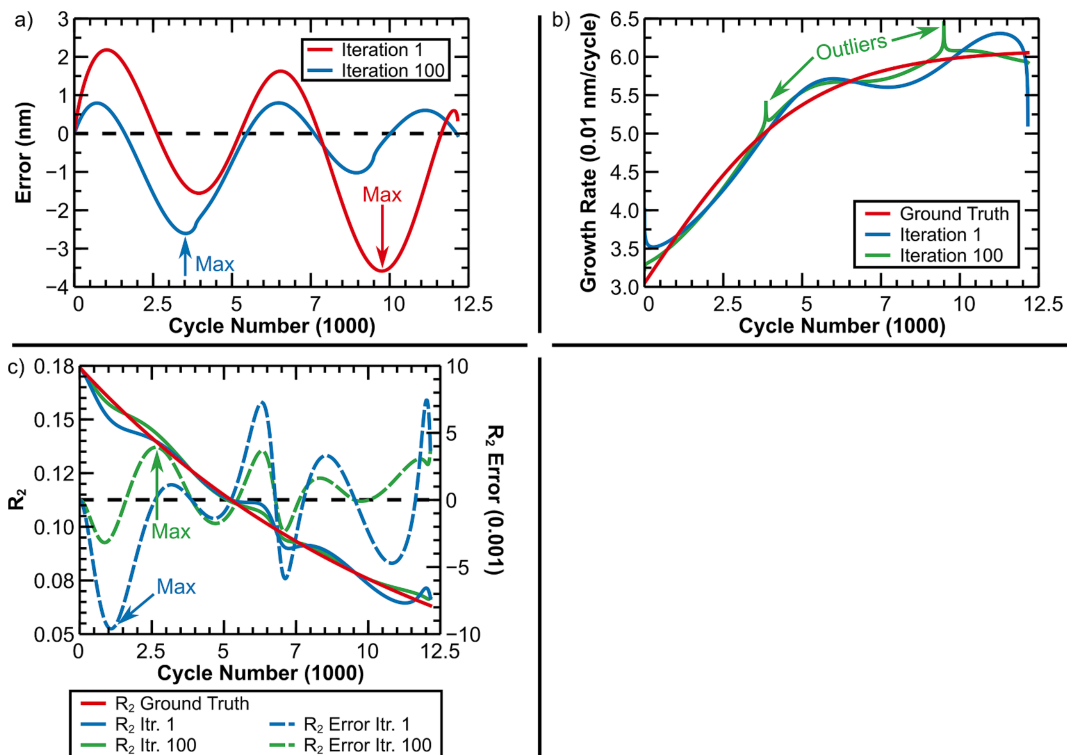


**Fig.9.** Comparison of film thickness, growth rate, and reflectivity of Interface 2 with those of the ground truth and the first iteration.

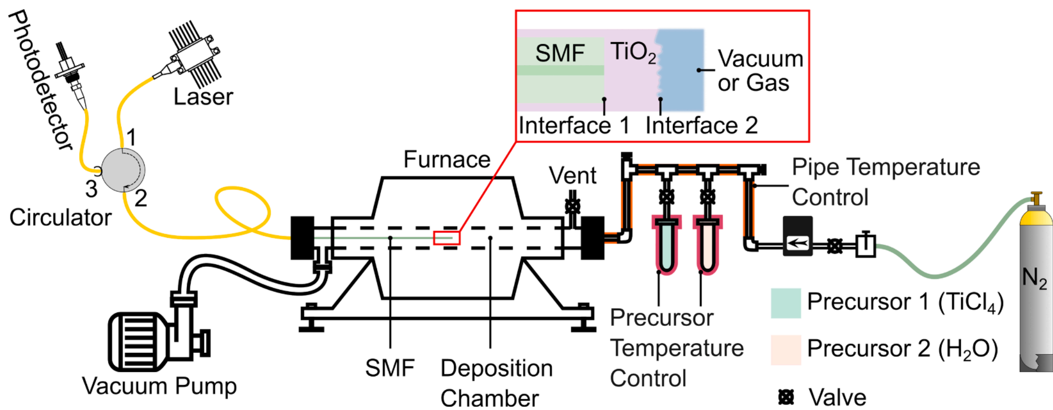


**Fig.10.** Thin film growth monitoring system using an optical fiber sensor.

**Table 1**
Test conditions and their corresponding recipes.

| Test # | Pressure (Pa) | Temperature (°C) | | | Time (sec) | | | |
|---|---|---|---|---|---|---|---|---|
| | | Furnace | Pipe | Precursor | Dose 1 | Purge 1 | Dose 2 | Purge 2 |
| 4 | 1.120 | 150 | 50 | 50 | 0.5 | 2.0 | 0.2 | 2.0 |
| 5 | 1.173 | 150 | 50 | 50 | 0.5 | 2.0 | 0.2 | 2.0 |
| 8 | 7.333 | 180 | 50 | 50 | 0.5 | 2.0 | 0.5 | 2.0 |
| 9 | 4.800 | 180 | 50 | 50 | 0.5 | 1.5 | 0.5 | 1.5 |

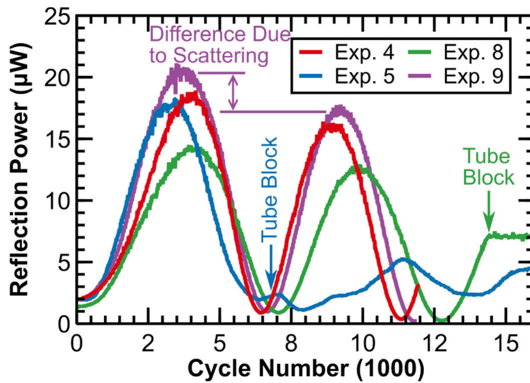


$\lambda$ = 1550 nm
$n$ = 2.4328
First Maximum: $\lambda/(4n)$ = 159.28 nm
First Minimum: $2\lambda/(4n)$ = 318.56 nm
Second Maximum: $3\lambda/(4n)$ = 477.84 nm
Second Minimum: $4\lambda/(4n)$ = 637.13 nm

**Fig.11.** Thin film interference monitoring and anomaly detection.

each maximum and minimum with the knowledge of the refractive index of $TiO_2$ at 1550 nm. For ideal condition, which does not have absorption and scattering of the thin film, the power of all the maximums and minimums should be the same. However, when propagating in the thin film, part of the light will be absorbed by the film. Also, due to the surface roughness of the interfaces, part of light will be scattered. These will cause a reduce of the maximums and minimums as shown in Fig. 11. Therefore, determining the film thickness is not easy by only observing the intensity at one single point. The maximums and minimums give a more accurate calculation of the film thickness. For test 5, a clog of the tube was found after inspection, which is the reason that the reflection power looks unusual after 7068 cycles (blue arrow). The same clog was also observed at experiment 8 (green arrow) where a complete stop of deposition was observed. This clog was caused by the accumulation of $TiO_2$ at the Tee joint.

In Fig. 11, the interval between the minimum reflection power and the next maximum reflection power with the increase of the cycle number will be called as the raising interval in this paper, and the interval between the maximum reflection power and the next minimum reflection power with the increase of the cycle number is called the falling interval. These intervals, including raising and falling, are numbered incrementally from number 1 and labeled as raising/falling interval $i$. For example, the first raising interval between cycle number 0 and the first peak is labeled as raising/falling interval 1, and the first falling interval between the first maximum and the next minimum is labeled as raising/falling interval 2. According to the cycle number of each raising/falling interval and the film thickness at the maxima and minima given in Fig. 11, the average growth rate can be calculated for each raising/falling interval as shown in Fig. 12. Here, we count each raising or falling interval from left of the interferogram in Fig. 11. As we can see, for

the first interval (raising), the film growth at a relatively lower rate between 0.034 nm/cycle and 0.047 nm/cycle. Start at the second interval, the growth rate tends to be constant within a range of 0.053 nm/cycle to 0.065 nm/cycle. The growth rate after the second interval agrees with the data published in Ref. [38].

Fig. 13 shows the film thickness and the growth rate of the $TiO_2$ deposition process of Exp. 9. Fig. 13 a) shows the maximum difference of film thickness between two neighboring iterations. As we can see, after 6 iterations, the difference is zero. Fig. 13 b) shows the film thickness, growth rate, and the surface roughness given by the calculation. The cross mark shows the film thickness calculated by the maximums and minimums of the interferogram. The red curve shows the film thickness, and the blue curve shows the growth rate. As we can see, the slope of the film thickness increases gradually from 0 to about 4000 cycles. Then, the slope remains constant with an insignificant fluctuation. The cross mark also shows the film thickness calculated from the maximums and minimums. As we can see, they agree well with the iteration results. The growth rate was calculated from taking derivative of the film thickness. As discussed in section 3.1, the growth rate wiggles around the true value. The film grows at a lower growth rate at the beginning, then it increases and after around 4000 cycles keeps to a relatively stable value. The growth rate stables at around 0.06 nm/cycle, which also agrees with Ref. [38]. The green curve shows the surface roughness of Interface 2 calculated from $R_2$ based on Eq. (12). As we can see, during the growth process, the surface roughness gradually increased and reached 95 nm at the end of the deposition process. To further evaluate the error between the proposed method and the widely accepted method by calculating the thickness using the maxima and minima of the interferogram, the thickness of the maxima and minima of the four experiments shown in Fig. 11 was calculated and shown in the box plot in Fig. 13 b). As we can see, the maximum and minimum differences are 4 nm and 0 nm, respectively. The average error is 1.67 nm, and the middle error is 1.00 nm. The standard deviation of the measurements is 1.43 nm. Among all the measurements, only two points have an error of 4 nm, all the rest points have an error smaller than or equal to 3 nm.

## 4. Conclusion

This research introduced an innovative method to monitor the growth process of a thin film deposited on the tip of a single mode optical fiber. Hilbert Transform was used to calculate the instantaneous phase of the interferogram. It was proved that the mapping from the instantaneous phase to the film thickness is a one-to-one mapping, ensuring the existence and uniqueness of the film thickness corresponding to an instantaneous phase. Furthermore, this research developed a method to calculate the film thickness and surface roughness when the reflectivity of the thin film-vacuum/gas interface changes during the growing process. In this method, assumption of optical smooth film-vacuum/gas interface ($R_2$) was used for the first iteration. Subsequently, the error caused by this assumption is gradually reduced by taking the calculated reflectivity of film-vacuum/gas interface as the input to recalculate the film thickness and the reflectivity $R_2$. According to the simulation results, the film thickness calculated using the proposed method fluctuates around the true value with an error on the nanometer scale ($\leq$4 nm in the numerical test). The growth rate and $R_2$ were calculated from film thickness with an error of lower than 0.004 in the numerical test. Additionally, with the information on $R_2$, the surface roughness of the film-vacuum/gas interface was calculated. The proposed method solves the following problems, having the following improvements compared with other methods such as quartz crystal microbalance or optics methods:

1. Simultaneously monitoring of both film thickness and surface roughness during the deposition process of transparent thin films.
2. Improves the monitoring accuracy compared to the direct implementation of Hilbert Transform by using an iterative approach.
3. Compared to the traditional quartz crystal microbalance method, it is compact in size, cost-effective, and provides direct and high-fidelity measurement of film thickness.
4. Unlike other optical methods, no complicated optical system or complex sensing structure are required.

Taken all together, the proposed method offers the potential for monitoring of the thin film growth processes in an affordable, time

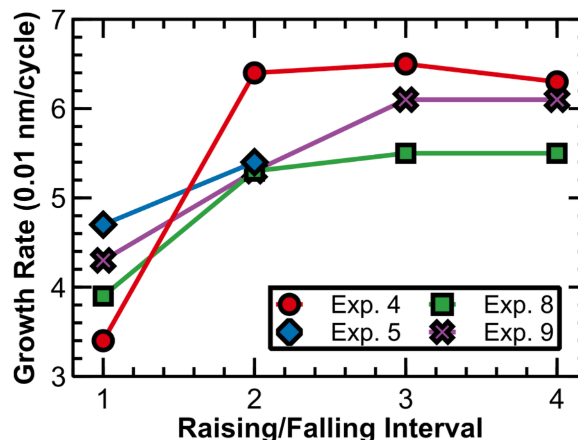


**Fig.12.** Average growth rate of each raising/falling period.

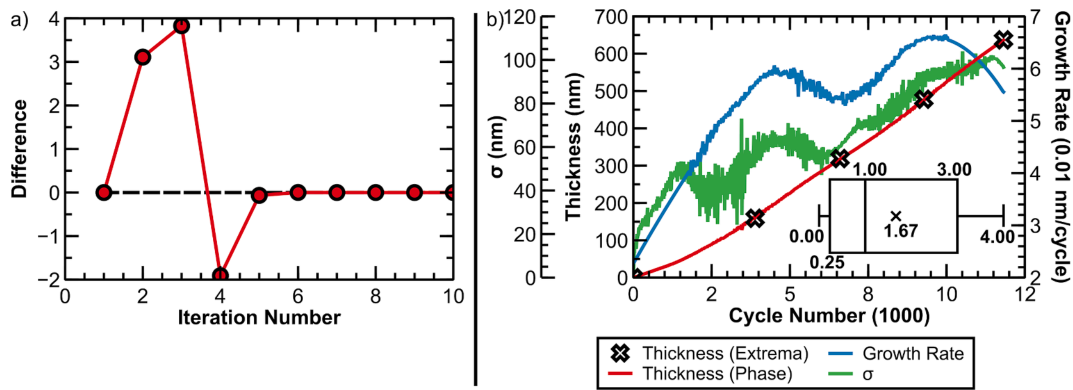


**Fig.13.** Monitoring results of the thin film growing process. a) maximum difference in film thickness between two consecutive iterations; b) thickness, growth rate, and surface roughness throughout the film growth process. The box plot in b) shows the statistics of error for the 4 experiments between the proposed method and the method using extrema.

efficient, and high-fidelity manner, with applications in optical coating monitoring, semiconductor manufacturing, and other emerging areas requiring quality control and understanding the deposition processes.

## CRediT authorship contribution statement

**Fengfeng Zhou:** Conceptualization, Formal analysis, Methodology, Validation, Writing – original draft, Writing – review & editing. **Siying Chen:** Data curation, Methodology, Writing – review & editing, Visualization. **Semih Akin:** Writing – review & editing, Validation, Supervision. **Theodore Gabor:** Writing – review & editing, Resources, Formal analysis. **Martin B.G. Jun:** Conceptualization, Writing – review & editing, Supervision, Funding acquisition, Project administration.

## Funding

This work was supported by the National Science Foundation under Grant No. NSF AM-2125826.

## Declaration of competing interest

The authors declare that they have no known competing financial interests or personal relationships that could have appeared to influence the work reported in this paper.

## Acknowledgements

This material is based upon work supported by the National Science Foundation under Grant No. NSF AM-2125826.

## Appendix

### A. Nomenclature

| | |
|---|---|
| $a$ | parameter, $a = 1$. |
| $b$ | parameter, $b = -T_1T_2$. |
| $c$ | parameter, $c = 1 + R_1R_2$. |
| $C$ | cycle number of the ALD process. |
| $d$ | parameter, $d = 2\sqrt{R_1R_2}$. |
| $g$ | the Intrinsic Mode Function of the analytical spectrum $I$. |
| $h$ | the mapping that maps the spectrum of the FPI to cosine function. |
| $h_r$ | the same as $h$ that maps the experimental spectrum of the FPI to a function. |
| $I$ | analytic spectrum of the FPI. |
| $I_e$ | the experimental interferogram. |
| $I_r$ | reflection intensity of the FPI. |
| $\widetilde{I}_r$ | Hilbert Transform of the reflection intensity $I_r$. |
| $\widetilde{I}$ | the imagine part of the analytical spectrum shifted by the IMF. |
| $I'$ | the real part of analytical spectrum shifted by the IMF. |

(continued on next page)

(*continued*)

| | |
|---|---|
| $l_0$ | geometric distance between two reflection interfaces. |
| $l_{0r}$ | estimation of thin film thickness calculated from an experimental spectrum using the proposed method. |
| $n_i$ | refractive index of material *i*. |
| $p$ | the instantaneous phase. |
| $p_d$ and $q_d$ | parameters between the maximum growth rate and the growth rate of the ALD process. |
| $p_i$ | the instantaneous phase given by the mapped experimental spectrum of the FPI. |
| $R_{20}$ | reflectivity of interface 2 with a smooth surface. |
| $R_i$ | reflectivity of interface *i*. |
| $s$ | parameter, $s = 4\pi n_2/\lambda_0$. |
| $T_i$ | transmissivity of interface *i*. |
| $v_M$ | the maximum growth rate of the ALD process in simulation, nm/cycle. |
| $v$ | the growth rate of the ALD process, nm/cycle. |
| $w$ | parameters between the reflectivity of the rough surface and the smooth surface of interface 2. |
| $\varphi$ | phase change when light travels between Interface 1 and Interface 2 for a roundtrip. |
| $\lambda_0$ | wavelength of the light in vacuum. |
| $\sigma$ | the surface roughness. |

## B. Calculation of refractive index of Interface 2

To calculate $R_2$, Eq. (9) may yield two solutions, some of which could complex. We need to identify the proper solution which does not violate physical law. The solution of $\sqrt{R_2}$ is:

$$\sqrt{R_2} = \frac{C_2 \pm \sqrt{C_2^2 - 4A_2B_2}}{2B_2}, \# \tag{A1}$$

where:

$$\begin{cases} A_2 = \dfrac{R_1 - I_r}{2(1-I_r)\sqrt{R_1}}, \\ B_2 = \dfrac{1 - R_1 I_r}{2(1-I_r)\sqrt{R_1}}, \\ C_2 = \cos(sl_0). \end{cases} \# \tag{A2}$$

First, consider the situation that $A_2B_2 \le 0$, which corresponds to $I_r \ge R_1$. We have the term under the square root:

$$\frac{C_2^2 - 4A_2B_2}{4B_2^2} = \frac{I_r(1-R_1)^2 - R_1(1-I_r)^2\sin^2(sl_0)}{(1-R_1I_r)^2}. \# \tag{A3}$$

Consider the worst condition that $\sin^2(sl_0) = 1$, we have the numerator of Eq. (A3) equals:

$$(I_r - R_1)(1 - I_rR_1) \ge 0. \# \tag{A4}$$

Therefore, real solutions for this condition exist. And consider the reasonable range of $\sqrt{R_2}$ is $\sqrt{R_2} \in (0,1)$, to avoid negative $\sqrt{R_2}$, we only need to consider if the following situation can be satisfied:

$$f_{R2} = \frac{C_2 + \sqrt{C_2^2 - 4A_2B_2}}{2B_2} < 1. \# \tag{A5}$$

Substitute Eq. (A2) into Eq. (A5), we have:

$$f_{R2} = \frac{(1-I_r)\sqrt{R_1}}{1-R_1I_r}\cos(sl_0) + \sqrt{\frac{I_r(1-R_1)^2 - R_1(1-I_r)^2\sin^2(sl_0)}{(1-R_1I_r)^2}}. \# \tag{A6}$$

Consider the worst situation that $\sin^2(sl_0) = 0$ and $\cos(sl_0) = 1$, we have:

$$f_{R2} < \frac{(1-I_r)\sqrt{R_1}}{1-R_1I_r} + \sqrt{\frac{I_r(1-R_1)^2}{(1-R_1I_r)^2}} = \frac{\sqrt{R_1} + \sqrt{I_r}}{1 + \sqrt{R_1I_r}}. \# \tag{A7}$$

Consider:

$$\left(1 + \sqrt{R_1I_r}\right) - \left(\sqrt{R_1} + \sqrt{I_r}\right) = \left(1 - \sqrt{I_r}\right)\left(1 - \sqrt{R_1}\right) > 0. \# \tag{A8}$$

We have:

$$f_{R2} < \frac{\sqrt{R_1} + \sqrt{I_r}}{1 + \sqrt{R_1 I_r}} < 1.\# \tag{A9}$$

Therefore, we have:

$$\frac{C_2 + \sqrt{C_2^2 - 4A_2B_2}}{2B_2} \in (0,1)\# \quad 10)$$

will always be satisfied, and this conclusion does not rely on the sign of $A_2B_2$. So, Eq. (A10) is the only solution when $A_2B_2 < 0$.
Now, for the situation that $A_2B_2 > 0$, which corresponds to $I_r < R_1$. First, consider the term under the square root:

$$f_I(I_r) = \frac{C_2^2 - 4A_2B_2}{4B_2^2} = \frac{I_r(1-R_1)^2 - R_1(1-I_r)^2\sin^2(sl_0)}{(1-R_1I_r)^2}.\# \quad 11)$$

As $f_I(I_r)$ increases monotonically, if $I_r$ is lower than the ideal value (optically smooth Interface 2) due to scattering, $C_2^2 - 4A_2B_2$ may become negative. In this case, we need to set $C_2^2 - 4A_2B_2 = 0$ to obtain real solutions. This adjustment will also correct the value of $R_2$, as valid $R_2$ should always yield a solution.

When $A_2B_2 > 0$, it is easy to prove that

$$\frac{C_2 - \sqrt{C_2^2 - 4A_2B_2}}{2B_2} \in (0,1)\# \quad 12)$$

will also be satisfied automatically since $C_2 > \sqrt{C_2^2 - 4A_2B_2}$ and

$$\frac{C_2 - \sqrt{C_2^2 - 4A_2B_2}}{2B_2} < \frac{C_2 + \sqrt{C_2^2 - 4A_2B_2}}{2B_2} < 1.\# \quad 13)$$

Therefore, Eq. (9) has two real solutions for $\sqrt{R_2}$. To choose the reasonable $\sqrt{R_2}$, we need to assume the surface roughness changes continuously with the growth of the thin film. Therefore, the reflectivity $R_2$ will also change continuously. Consider the solution of $\sqrt{R_2}$ is given by Eq. (A10) when $A_2B_2 < 0$, we should choose the same solution for $A_2B_2 > 0$. Therefore, we have:

$$R_2 = \left\{ Re\left[\frac{C_2 + \sqrt{C_2^2 - 4A_2B_2}}{2B_2}\right]\right\}^2.\# \quad 14)$$

## C. Influence of $R_2$ to the maxima and minima of the interferogram

Since $R_2$ may change during the monitoring process due to the variations in the surface roughness of the thin film, we need to determine whether changes in $R_2$ affect the maxima and minima of the interferogram. Rewriting Eq. (1), we have:

$$I_r = \frac{R_1 + R_2 - 2\sqrt{R_1R_2}\cos(sl_0)}{1 + R_1R_2 - 2\sqrt{R_1R_2}\cos(sl_0)}.\# \quad 15)$$

Consider the interferogram with $l_0$ as variable, take derivative of $I_r$ with respect to $l_0$:

$$\frac{\partial I_r}{\partial l_0} = \frac{2s(1-R_1)(1-R_2)\sqrt{R_1R_2}\sin(sl_0)}{\left[1 + R_1R_2 - 2\sqrt{R_1R_2}\cos(sl_0)\right]^2}.\# \quad 16)$$

For the denominator, we have:

$$1 + R_1R_2 - 2\sqrt{R_1R_2}\cos(sl_0) = \left(1 - \sqrt{R_1R_2}\right)^2 + 2\sqrt{R_1R_2}[1 - \cos(sl_0)] > 0.\# \quad 17)$$

The numerator equals to zero only when $\sin(sl_0) = 0$. Therefore, change in $R_2$ will not affect the maxima and minima in the interferogram.

## Data availability

Data will be made available on request.

## References


[1] L. Li, X. Yu, Z. Lin, Z. Cai, Y. Cao, W. Kong, Z. Xiang, Z. Gu, X. Xing, X. Duan, Y. Song, Interface capture effect printing atomic-thick 2D semiconductor thin films, Adv. Mater. 34 (2022) 2207392, https://doi.org/10.1002/adma.202207392.

[2] I. Ohkubo, M. Murata, M.S.L. Lima, T. Sakurai, Y. Sugai, A. Ohi, T. Aizawa, T. Mori, Miniaturized in-plane π-type thermoelectric device composed of a II–IV semiconductor thin film prepared by microfabrication, Mater. Today Energy 28 (2022) 101075, https://doi.org/10.1016/j.mtener.2022.101075.

[3] S. Lee, L. Ji, A.C. De Palma, E.T. Yu, Scalable, highly stable Si-based metal-insulator-semiconductor photoanodes for water oxidation fabricated using thin-film reactions and electrodeposition, Nat. Commun. 12 (2021) 3982, https://doi.org/10.1038/s41467-021-24229-y.

[4] D. Zhu, L. Shao, M. Yu, R. Cheng, B. Desiatov, C.J. Xin, Y. Hu, J. Holzgrafe, S. Ghosh, A. Shams-Ansari, E. Puma, N. Sinclair, C. Reimer, M. Zhang, M. Lončar, Integrated photonics on thin-film lithium niobate, Adv. Opt. Photon., AOP 13 (2021) 242–352, https://doi.org/10.1364/AOP.411024.

[5] J. Holzgrafe, N. Sinclair, D. Zhu, A. Shams-Ansari, M. Colangelo, Y. Hu, M. Zhang, K.K. Berggren, M. Lončar, Cavity electro-optics in thin-film lithium niobate for efficient microwave-to-optical transduction, Optica 7 (2020) 1714–1720, https://doi.org/10.1364/OPTICA.397513.

[6] M. Xu, M. He, H. Zhang, J. Jian, Y. Pan, X. Liu, L. Chen, X. Meng, H. Chen, Z. Li, X. Xiao, S. Yu, S. Yu, X. Cai, High-performance coherent optical modulators based on thin-film lithium niobate platform, Nat. Commun. 11 (2020) 3911, https://doi.org/10.1038/s41467-020-17806-0.

[7] P. Oldroyd, J. Gurke, G.G. Malliaras, Stability of thin film neuromodulation electrodes under accelerated aging conditions, Adv. Funct. Mater. 33 (2023) 2208881, https://doi.org/10.1002/adfm.202208881.

[8] J.W. Park, B.H. Kang, H.J. Kim, A review of low-temperature solution-processed metal oxide thin-film transistors for flexible electronics, Adv. Funct. Mater. 30 (2020) 1904632, https://doi.org/10.1002/adfm.201904632.

[9] R. Luo, H. Fu, Y. Li, Q. Xing, G. Liang, P. Bai, X. Guo, J. Lyu, M. Tsapatsis, In situ fabrication of metal–organic framework thin films with enhanced pervaporation performance, Adv. Funct. Mater. 33 (2023) 2213221, https://doi.org/10.1002/adfm.202213221.

[10] A.S. Patil, R.D. Waghmare, S.P. Pawar, S.T. Salunkhe, G.B. Kolekar, D. Sohn, A.H. Gore, Photophysical insights of highly transparent, flexible and re-emissive PVA @ WTR-CDs composite thin films: a next generation food packaging material for UV blocking applications, J. Photochem. Photobiol. A Chem. 400 (2020) 112647, https://doi.org/10.1016/j.jphotochem.2020.112647.

[11] A. Khlyustova, Y. Cheng, R. Yang, Vapor-deposited functional polymer thin films in biological applications, J. Mater. Chem. B 8 (2020) 6588–6609, https://doi.org/10.1039/D0TB00681E.

[12] K.-Y. Chan, D.Q. Pham, B. Demir, D. Yang, E.L.H. Mayes, A.P. Mouritz, A.S.M. Ang, B. Fox, H. Lin, B. Jia, K.-T. Lau, Graphene oxide thin film structural dielectric capacitors for aviation static electricity harvesting and storage, Compos. B Eng. 201 (2020) 108375, https://doi.org/10.1016/j.compositesb.2020.108375.

[13] S.D. Ponja, S. Sathasivam, I.P. Parkin, C.J. Carmalt, Highly conductive and transparent gallium doped zinc oxide thin films via chemical vapor deposition, Sci. Rep. 10 (2020) 638, https://doi.org/10.1038/s41598-020-57532-7.

[14] K. Natu, M. Laad, B. Ghule, A. Shalu, Transparent and flexible zinc oxide-based thin-film diodes and thin-film transistors: a review, J. Appl. Phys. 134 (2023) 190701, https://doi.org/10.1063/5.0169308.

[15] Y. Wang, Y. Li, Z. Li, L. Ren, Large-scale plasma-polymerized hexamethyldisiloxane thin films: role of interelectrode distance and excellent corrosion resistance, ACS Appl. Mater. Interfaces 14 (2022) 56169–56175, https://doi.org/10.1021/acsami.2c18312.

[16] F. Larsson, L. Stolt, A. Hultqvist, M. Edoff, J. Keller, T. Törndahl, Atomic layer deposition of ternary compounds on Cu(In,Ga)Se2: an in situ quartz crystal microbalance study, ACS Appl. Energy Mater. 3 (2020) 7208–7215, https://doi.org/10.1021/acsaem.0c01284.

[17] X. Zhao, H. Gao, Y. Hou, L. Gbologah, X. Zeng, Y. Wang, Analysis of crystallization and deposition process using electrochemical-quartz crystal microbalance: a review, J. Electroanal. Chem. 904 (2022) 115936, https://doi.org/10.1016/j.jelechem.2021.115936.

[18] P. Niiranen, H. Nadhom, M. Zanáška, R. Boyd, M. Sortica, D. Primetzhofer, D. Lundin, H. Pedersen, Biased quartz crystal microbalance method for studies of chemical vapor deposition surface chemistry induced by plasma electrons, Rev. Sci. Instrum. 94 (2023) 023902, https://doi.org/10.1063/5.0122143.

[19] A. Rosental, P. Adamson, A. Gerst, A. Niilisk, Monitoring of atomic layer deposition by incremental dielectric reflection, Appl. Surf. Sci. 107 (1996) 178–183, https://doi.org/10.1016/S0169-4332(96)00483-7.

[20] F. Zhou, P. Kung, X. Li, V. Behjat, M.B.G. Jun, Modeling of a sampled apodized fiber Bragg grating moisture sensor, Opt. Fiber Technol. 65 (2021) 102630, https://doi.org/10.1016/j.yofte.2021.102630.

[21] F. Zhou, S. Jo, X. Fu, J.-T. Tsai, M.B.-G. Jun, Fabrication of Optical Fiber Sensors Based on Femtosecond Laser Micro Machining, (n.d.) 28.

[22] F. Zhou, X. Fu, S. Chen, E. Kim, M.-B.-G. Jun, Fiber optic sensor for smart manufacturing, Int. J. Precis. Eng. Manuf. 1 (2023) 125–136.

[23] X. Fu, F. Zhou, H. Yun, E. Kim, S. Chen, M.-B.-G. Jun, Machine straightness error measurement based on optical fiber Fabry–Pérot interferometer monitoring technique, J. Manuf. Sci. Eng. 145 (2023) 011007.

[24] F. Zhou, W. Duan, X. Li, J.-T. Tsai, M.B.G. Jun, High precision in-situ monitoring of electrochemical machining process using an optical fiber Fabry–Pérot interferometer sensor, J. Manuf. Process. 68 (2021) 180–188, https://doi.org/10.1016/j.jmapro.2021.07.010.

[25] F. Zhou, J.-T. Tsai, S. Jo, G. Kim, P.C. Lee, M.-B.-G. Jun, In-situ monitoring of solidification process of PVA solution by fiber optic sensor technique, IEEE Sens. J. (2020) 1, https://doi.org/10.1109/JSEN.2020.3040571.

[26] F. Zhou, S. Chen, X. Fu, M.B.G. Jun, Real-time monitoring of the interelectrode gap during electrochemical machining processes using a smart machine tool equipped with an optical fiber Fabry-Pérot interferometer: Principle and application, Mech. Syst. Sig. Process. 211 (2024) 111245, https://doi.org/10.1016/j.ymssp.2024.111245.

[27] F. Zhou, X. Fu, S. Chen, C. Han, M. Jun, 3D profile reconstruction and internal defect detection of silicon wafers using cascaded fiber optic Fabry-Pérot interferometer and leaky field detection technologies, J. Manuf. Sci. Eng. (2024) 1–11, https://doi.org/10.1115/1.4065523.

[28] H.E. Joe, F. Zhou, S.T. Yun, M.B.G. Jun, Detection and quantification of underground CO2 leakage into the soil using a fiber-optic sensor, Opt. Fiber Technol. 60 (2020) undefined-undefined, https://doi.org/10.1016/j.yofte.2020.102375.

[29] F. Zhou, H. Su, H.-E. Joe, M.B.-G. Jun, Temperature insensitive fiber optical refractive index probe with large dynamic range at 1,550 nm, Sensors and Actuators A: Physical (2020) 112102.

[30] R. Min, Z. Liu, L. Pereira, C. Yang, Q. Sui, C. Marques, Optical fiber sensing for marine environment and marine structural health monitoring: a review, Opt. Laser Technol. 140 (2021) 107082.

[31] M. Born, E. Wolf, Principles of Optics, 7th (expanded) edition, United Kingdom: Press Syndicate of the University of Cambridge 461 (1999).

[32] N. Ismail, C.C. Kores, D. Geskus, M. Pollnau, Fabry-Pérot resonator: spectral line shapes, generic and related Airy distributions, linewidths, finesses, and performance at low or frequency-dependent reflectivity, Opt. Express 24 (2016) 16366–16389.

[33] J. Kischkat, S. Peters, B. Gruska, M. Semtsiv, M. Chashnikova, M. Klinkmüller, O. Fedosenko, S. Machulik, A. Aleksandrova, G. Monastyrskyi, others, Mid-infrared optical properties of thin films of aluminum oxide, titanium dioxide, silicon dioxide, aluminum nitride, and silicon nitride, Appl. Opt. 51 (2012) 6789–6798.

[34] I.H. Malitson, Interspecimen comparison of the refractive index of fused silica*,†, J. Opt. Soc. Am., JOSA 55 (1965) 1205–1209, https://doi.org/10.1364/JOSA.55.001205.

[35] C.Z. Tan, Determination of refractive index of silica glass for infrared wavelengths by IR spectroscopy, J. Non Cryst. Solids 223 (1998) 158–163, https://doi.org/10.1016/S0022-3093(97)00438-9.

[36] H.E. Bennett, J.O. Porteus, Relation between surface roughness and specular reflectance at normal incidence, J. Opt. Soc. Am., JOSA 51 (1961) 123–129, https://doi.org/10.1364/JOSA.51.000123.

[37] N.E. Huang, Z. Shen, S.R. Long, M.C. Wu, H.H. Shih, Q. Zheng, N.-C. Yen, C.C. Tung, H.H. Liu, The empirical mode decomposition and the Hilbert spectrum for nonlinear and non-stationary time series analysis, in: Proceedings of the Royal Society of London. Series a: Mathematical, Physical and Engineering Sciences, 1998, pp. 903–995, https://doi.org/10.1098/rspa.1998.0193.

[38] J. Aarik, A. Aidla, H. Mändar, T. Uustare, Atomic layer deposition of titanium dioxide from TiCl4 and H2O: investigation of growth mechanism, Appl. Surf. Sci. 172 (2001) 148–158, https://doi.org/10.1016/S0169-4332(00)00842-4.